

Characteristic mode analysis of wideband high-gain and low-profile metasurface antenna

Kun Gao(高坤), Xiang-Yu Cao(曹祥玉), Jun Gao(高军), Huan-Huan Yang(杨欢欢), and Jiang-Feng Han(韩江枫)
Citation: Chin. Phys. B, 2021, 30 (**6**): 064101. DOI: 10.1088/1674-1056/abdb23
Journal homepage: http://cpb.iphy.ac.cn; http://iopscience.iop.org/cpb

What follows is a list of articles you may be interested in

Ultra-wideband low radar cross-section metasurface and its application on waveguide slot antenna array

Li-Li Cong(丛丽丽), Xiang-Yu Cao(曹祥玉), Tao Song(宋涛), Jun Gao(高军)
Chin. Phys. B, 2018, 27 (**11**): 114101. DOI: 10.1088/1674-1056/27/11/114101

Design of multi-band metasurface antenna array with low RCS performance

Si-Ming Wang(王思铭), Jun Gao(高军), Xiang-Yu Cao(曹祥玉), Yue-Jun Zheng(郑月军), Tong Li(李桐), Jun-Xiang Lan(兰俊祥), Liao-Ri Ji-Di(吉地辽日)
Chin. Phys. B, 2018, 27 (**10**): 104102. DOI: 10.1088/1674-1056/27/10/104102

Ultra-broadband and polarization-independent planar absorber based on multilayered graphene

Jiao Wang(王娇), Chao-Ning Gao(高超宁), Yan-Nan Jiang(姜彦南), Charles Nwakanma Akwuruoha
Chin. Phys. B, 2017, 26 (**11**): 114102. DOI: 10.1088/1674-1056/26/11/114102

Ultra-wideband RCS reduction using novel configured chessboard metasurface

Ya-Qiang Zhuang(庄亚强), Guang-Ming Wang(王光明), He-Xiu Xu(许河秀)
Chin. Phys. B, 2017, 26 (**5**): 054101. DOI: 10.1088/1674-1056/26/5/054101

Design of ultra wideband microwave absorber effectual for objects of arbitrary shape

Gong Yuan-Xun, Zhou Zhong-Xiang, Jiang Jian-Tang, Zhao Hong-Jie
Chin. Phys. B, 2015, 24 (**12**): 124101. DOI: 10.1088/1674-1056/24/12/124101

Characteristic mode analysis of wideband high-gain and low-profile metasurface antenna*

Kun Gao(高坤)†, Xiang-Yu Cao(曹祥玉)‡, Jun Gao(高军), Huan-Huan Yang(杨欢欢), and Jiang-Feng Han(韩江枫)

Information and Navigation College of Air Force Engineering University, Xi'an 710077, *China*

(Received 6 October 2020; revised manuscript received 24 December 2020; accepted manuscript online 13 January 2021)

A wideband high-gain and low-profile metasurface antenna is proposed by analyzing characteristic quantities and parameters in the characteristic modes (CMs). The detailed modal current and modal weighting coefficient are analyzed to explain the broadband operation and high gain. A dominant characteristic mode is well excited, leading to a broadband operation. The mode behaviors of the excitation are changed to suppress the unwanted higher-order modes and improve the radiation performance by changing the widths of two patches. The measured impedance bandwidth for −10 dB is 39.8% (5.3 GHz–7.94 GHz) with a gain of 7.8 dBi–10.04 dBi over the operating bandwidth.

Keywords: characteristic mode analysis, wideband, high gain, metasurface antenna

PACS: 41.20.Jb, 73.20.Mf **DOI:** 10.1088/1674-1056/abdb23

1. Introduction

Microstrip patch antennas have been widely used in wireless communication, satellite communication for their excellent performances of low profile, easy conformal, and easy processing. Electromagnetic metasurface (MTS) provides the solutions to the inherent shortcomings such as low gain and narrow band, and greatly expands the performances, such as nano imaging,[1] phase modulation,[2–5] polarization conversion,[6,7] high performance,[8] *etc*. However, traditional MTS has limitations in application, and good MTS needs to be designed based on rich experience. The equivalent circuit theory,[9–11] effective medium theory,[12] surface impedance extraction,[13,14] and other theories have been used to characterize the MTS. But these methods are not suitable for MTS antenna analysis consisting of only a few units. The theory of characteristic mode (TCM) based on the method of moment (MOM) is a practical method of designing antenna, which can have an in-depth physical insight into the radiation phenomenon in the antenna. The TCM guides the design of MTS, and realizes the function of suppressing higher-order modes and exciting the desired modes to improve the radiation performance.[15] Recently, the TCM is used to analyze and optimize low-profile wideband metasurface antennas with microstrip feeding and coaxial feeding respectively.[16,17] In Ref. [18], the TCM is also used to analyze the orthogonal modal current with equal modal significance (MS) amplitude and phase difference of 90° to find the optimal feeding point position and realize circular polarization. In Ref. [19], a new combined characteristic mode (CM) associated with low resistance resonances of slot antenna is introduced to increase the bandwidth of ring slot antenna by loading stubs. In addition, according to the guidelines of modal weighting coefficient (MWC), a low RCS T-shaped slot antenna is designed to suppress the scattering mode while maintaining the radiation mode by loading reactance components and slots.[20] So far, a small amount of work has been done on the design of high gain antenna in wideband range based on characteristic mode analysis (CMA).

In this paper, a metasurface antenna is designed for wideband high-gain and low-profile operation based on the CMA. The antenna is comprised of a rectangle patch fed by coaxial probe sandwiched between the metasurface composed of three sizes and the ground plane. The CMs of the proposed and original metasurface are in depth analyzed in order to explain the working principle and study the underlying modal behaviors of the metasurface and guide the mode excitation. The designed metasurface antenna length is 0.065 λ_0 (λ_0 is the working wavelength of 6.5 GHz in free space). The designed antenna is in good agreement between simulation and measurement.

The rest of this paper is structured as follows. In Section 2, the characteristic mode theory of multilayered dielectric antenna is briefly introduced. In Section 3, the antenna structure is illustrated, the characteristic mode analysis of the proposed and original antenna are conducted, and the gain enhancement is analyzed. Section 4 reports the simulation of the antenna and the measurement environment. The final conclusions are given in Section 5.

*Project supported by the National Natural Science Foundation of China (Grant Nos. 61671464 and 61801508), the Postdoctoral Innovative Talents Support Program of China (Grant No. BX20180375), and the Natural Science Research Fund of Shaanxi Province, China (Grant No. 2019JQ-103).

†Corresponding author. E-mail: gkmicrowave@163.com

‡Corresponding author. E-mail: xiangyucaokdy@163.com

© 2021 Chinese Physical Society and IOP Publishing Ltd

2. TCM of multilayered medium

The theory of characteristic modes (TCM) was first introduced in 1965,[21] and in the few years that follows, it was further developed to analyze the radiation and scattering properties of dielectric and magnetic material bodies by the MOM.[22–25] The elements of the impedance matrix Z can be expressed by applying the standard Galerkin's procedure to the MPIE.[26,27] Following the procedure of the conventional TCM for PEC bodies, a generalized eigenvalue equation for the MPIE can be written as

$$XJ_n = \lambda_n RJ_n, \tag{1}$$

where R and X are the real part and imaginary part of the impedance matrix Z, respectively. λ_n is the real eigenvalue associated with each characteristic current J_n, and n denotes the index of the order of each mode. Characteristic modes form a complete set of solutions, and hence the total current can be expressed as a linear superposition of these mode currents

$$J = \sum_n \alpha_n J_n, \tag{2}$$

where α_n denotes the modal weighting coefficient (MWC) and can be calculated from

$$\alpha_n = \frac{V_n^{\mathrm{i}}}{1+\mathrm{j}\lambda_n} = \frac{\langle J_n, E^{\mathrm{i}}\rangle}{1+\mathrm{j}\lambda_n}, \tag{3}$$

where the term V_n^{i} is called the modal excitation coefficient (MEC), and E^{i} is the external excitation. The MS is expressed as

$$\mathrm{MS} = \left|\frac{1}{1+\mathrm{j}\lambda_n}\right|. \tag{4}$$

The mode resonates and radiates most efficiently when $\mathrm{MS} = 1$, that is, $\lambda_n = 0$. Suppressing unwanted modes requires reducing $|\alpha_n|$, or changing the unwanted modal current behaviors.

3. CMA of metasurface antenna

3.1. Antenna structure and design

The structure of the proposed antenna is shown in Fig. 1. The antenna consists of three metallic layers,a metasurface, a microstrip patch, and a ground from top to bottom. The two F4B substrates ($\varepsilon_{\mathrm{r}} = 2.65$ and $\tan\delta = 0.0007$) are both 1.5 mm in thickness. The metasurface is composed of three sizes of patches. It should be noted that the widths of the two patches adjacent to the center patch in the x direction are both S_{p} and the two ends of the patche in the y direction are square patches, with each side being W_{p}.

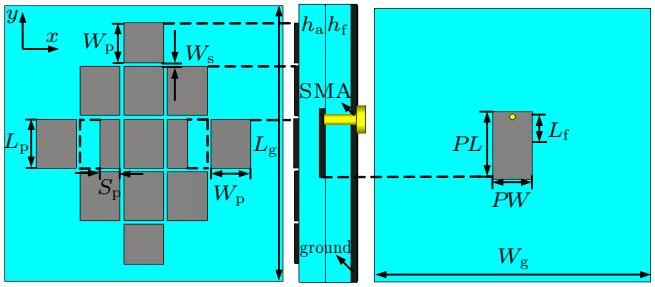


Fig. 1. Structure of proposed antenna, with $W_{\mathrm{g}} = 50$ mm, $L_{\mathrm{g}} = 50$ mm, $W_{\mathrm{p}} = 7.2$ mm, $L_{\mathrm{p}} = 8.9$ mm, $S_{\mathrm{p}} = 3.6$ mm, $W_{\mathrm{s}} = 0.65$ mm, $PW = 7.2$ mm, $PL = 12.3$ mm, $L_{\mathrm{f}} = 5.2$ mm, $h_{\mathrm{a}} = 1.5$ mm, and $h_{\mathrm{f}} = 1.5$ mm.

3.2. CMA of proposed antenna structure

The CMs are obtained using the MoM-based CMA tool in commercial simulation software CST Studio Suite 2020, in which the ground plane and dielectric layers extend infinitely by using a multilayer solver. The dielectric loss is neglected in the CMA but considered in the time domain analysis, and all other geometric dimensions of the antenna are kept unchanged.

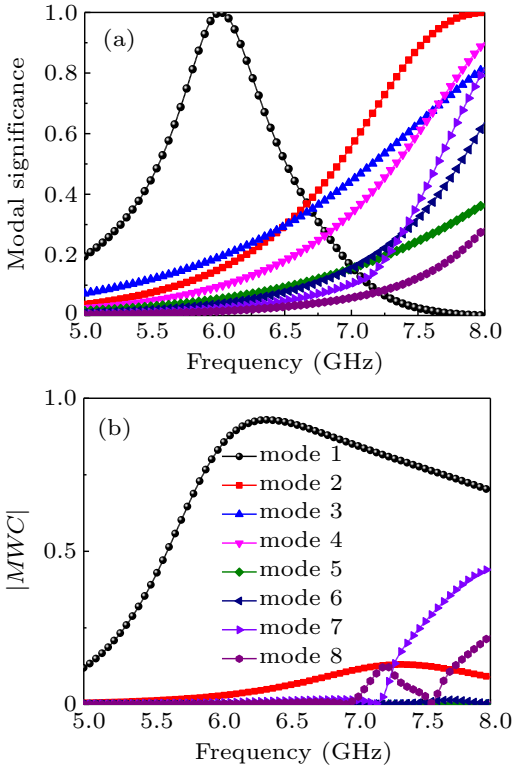


Fig. 2. (a) Modal significance and (b) $|MWC|$ *versus* frequency for several modes of antenna structure.

The calculated MS of the first eight modes of the proposed structure without the feed are plotted in Fig. 2(a). Modal currents and radiation patterns of J_1–J_8 are shown in Figs. 3 and 4, respectively. As can be seen, J_1 and J_7 are linearly polarized along the y axis with broadside radiation, while J_3 is linearly polarized along the x axis. J_2, J_4, and J_5 are symmetrical, and the patterns are split. J_6 is in the shape of a ring, which does not radiate outwards , and the main lobe of the mode pattern is concave. The J_8 is reversed in the x direction

and symmetrical in the y direction, and the side lobe level is higher. It can be seen that J_1 and J_7 are the modes that need to be excited, and the other modes are unwanted modes. The mode electric field on the microstrip patch is shown in Fig. 5. The feed point is marked with an empty circle. The coaxial feed is selected at the point where the modal E-field of the J_1 and J_7 are largest and the undesired mode excitation intensity is minimum. The coaxial probe fed by electric field coupling can be regarded as a capacitive coupling element (CCE).[28,29] If the CCE is placed at the peak of the J_1 and J_7, the desired modes will be greatly excited. The modal weighting coefficients (MWCs) of the first eight modes are obtained from Eq. (3) to measure the ratio of each mode's radiation power to the total radiation power as shown in Fig. 2(b). The excited mode current distribution is basically the same as that of the mode current without feed structure in Fig. 3. It can be seen that J_1 is dominant and J_7 is partially excited in the higher frequency band. Some unwanted modes are well suppressed due to the selection of appropriate feeding position. In addition, J_2 and J_8 are negligible compared with J_1 and J_7.

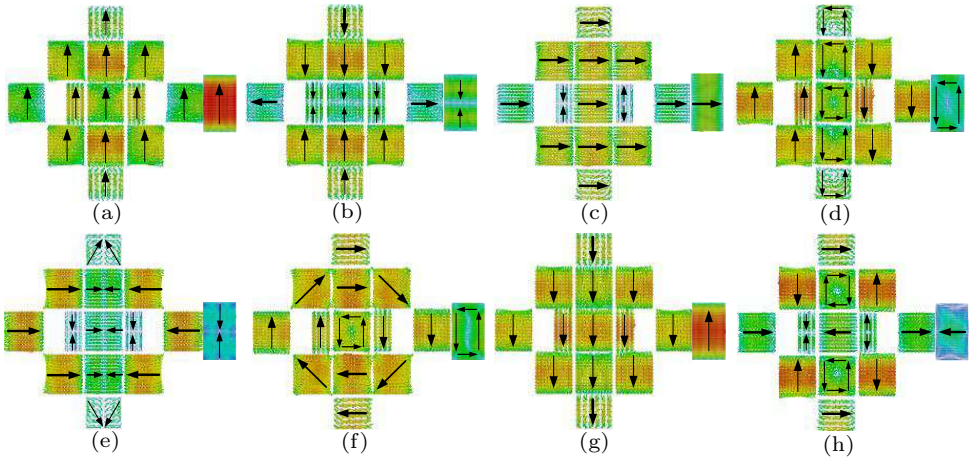


Fig. 3. Modal current distribution, for (a) J_1 at 6 GHz, (b) J_2 at 8 GHz, (c) J_3 at 8 GHz, (d) J_4 at 8 GHz, (e) J_5 at 8 GHz, (f) J_6 at 8 GHz, (g) J_7 at 8 GHz, and (h) J_8 at 8 GHz.

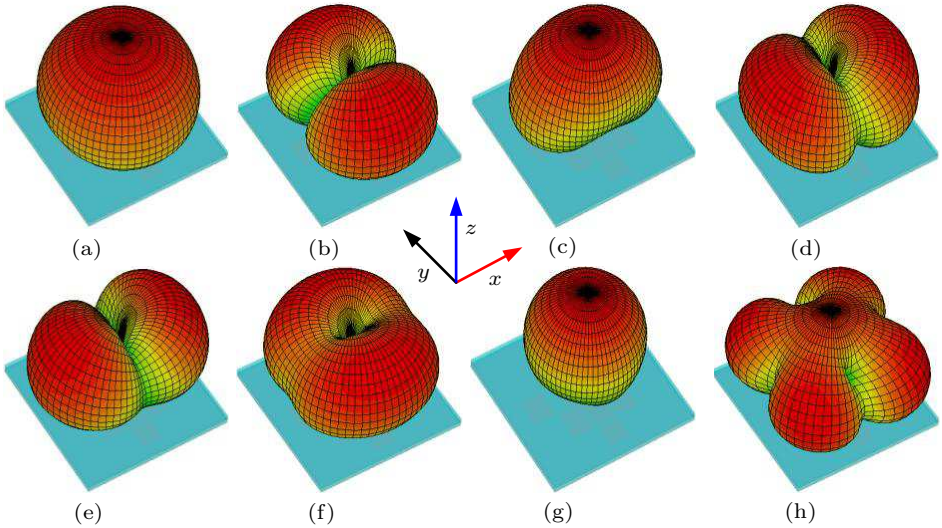


Fig. 4. Modal radiation patterns for (a) J_1 at 6 GHz, (b) J_2 at 8 GHz, (c) J_3 at 8 GHz, (d) J_4 at 8 GHz, (e) J_5 at 8 GHz, (f) J_6 at 8 GHz, (g) J_7 at 8 GHz, and (h) J_8 at 8 GHz.

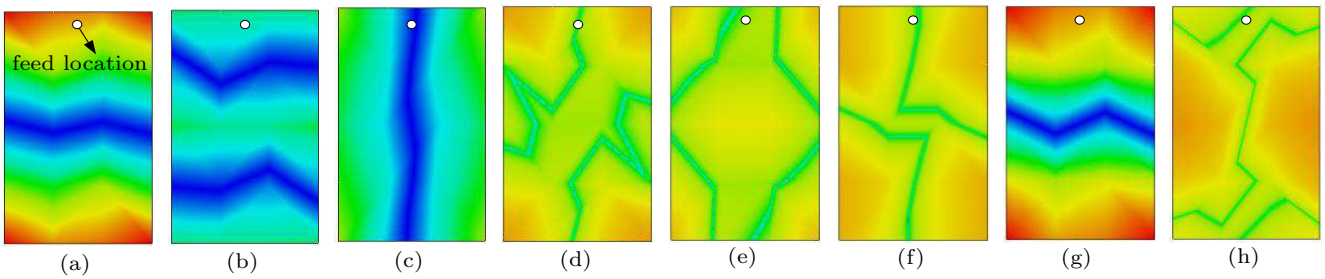


Fig. 5. Modal radiation patterns, for (a) J_1 at 6 GHz, (b) J_2 at 8 GHz, (c) J_3 at 8 GHz, (d) J_4 at 8 GHz, (e) J_5 at 8 GHz, (f) J_6 at 8 GHz, (g) J_7 at 8 GHz, and (h) J_8 at 8 GHz.

3.3. Gain enhancement analysis

The top view of the original antenna structure is shown in Fig. 6(a), and the geometric dimension is kept unchanged except S_p that is changed into 7.2 mm. The CMA is performed on the original antenna with the coaxial feed structure, and the mode with coaxial feed excitation is more consistent with the actual excitation mode for the origin antenna structure. The mode current is shown in Fig. 7, and MWC is shown in Fig. 6(b). The J_{s1} is dominant, while J_{s5} and J_{s7} are also excited to different degrees at high frequency. The J_{s5} is symmetrical, and J_{s7} is opposite to the current in the y direction of the center, which results in the large side lobe and the concave gain of the original antenna at high frequency. Figure 8 shows the reflection coefficient and gain *versus* frequency of the original antenna, as well as the pattern at 5.5 GHz, 6.5 GHz, and 7.5 GHz, separately. It can be seen that the pattern has a larger sidelobe and a concave gain at 7.5 GHz.

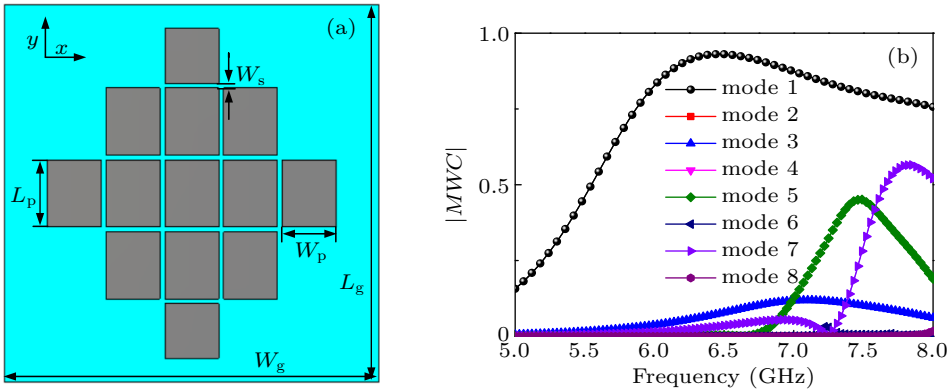


Fig. 6. (a) Top view of original antenna structure and (b) $|MWC|$ *versus* frequency for various modes of original antenna structure.

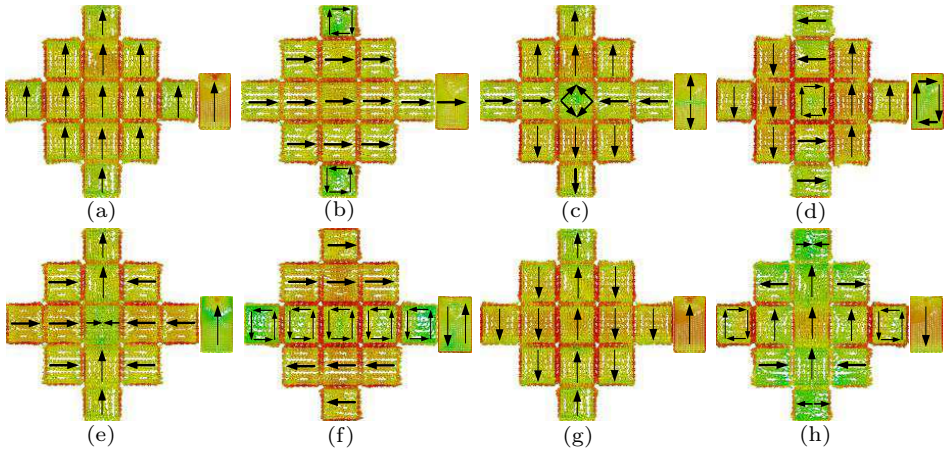


Fig. 7. Modal currents distribution of original antenna for (a) J_{s1} at 6 GHz, (b) J_{s2} at 8 GHz, (c) J_{s3} at 8 GHz, (d) J_{s4} at 8 GHz, (e) J_{s5} at 8 GHz, (f) J_{s6} at 8 GHz, (g) J_{s7} at 8 GHz, and (h) J_{s8} at 8 GHz.

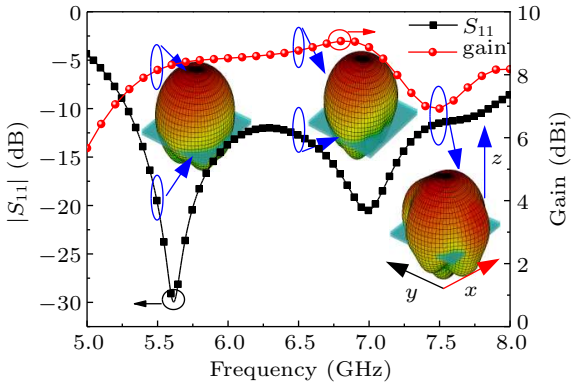


Fig. 8. Reflection coefficient and gain *versus* frequency of original antenna, and pattern at 5.5 GHz, 6.5 GHz, and 7.5 GHz.

In order to reduce the side lobe and enhance the gain, the patch named Spatch with width S_p in Fig. 1 plays a pivotal role in radiation performance, and the variations of impedance matching and gain with frequency for various values of S_p are studied as shown in Fig. 9. In the lower-end frequency band, the dominant mode current J_{s1} on the Spatch is in the identical direction with that on the center patch and the microstrip patch, and the boresight gain declines with S_p decreasing; in the upper-end frequency band, the higher-order mode current on the Spatch is different from that on the center patch and microstrip patch, and the boresight gain increases with S_p decreasing. Owing to the fact that the mode current on the Spatch cancels out the radiation, the gain drops sharply within 7 GHz–8 GHz, when S_p is 7.2 mm. When S_p is greater than 3.6 mm, the −10-dB impedance bandwidth is satisfactory, and

vice versa. The bandwidth is basically stable except for slight frequency shift. It is worth mentioning that the four corner patches and Spatch with 3.6 mm increase the antenna gain by 1.1 dB, and the two square patches expand the bandwidth. To summarize, S_p is chosen to be 3.6 mm, which can improve the radiation performance.

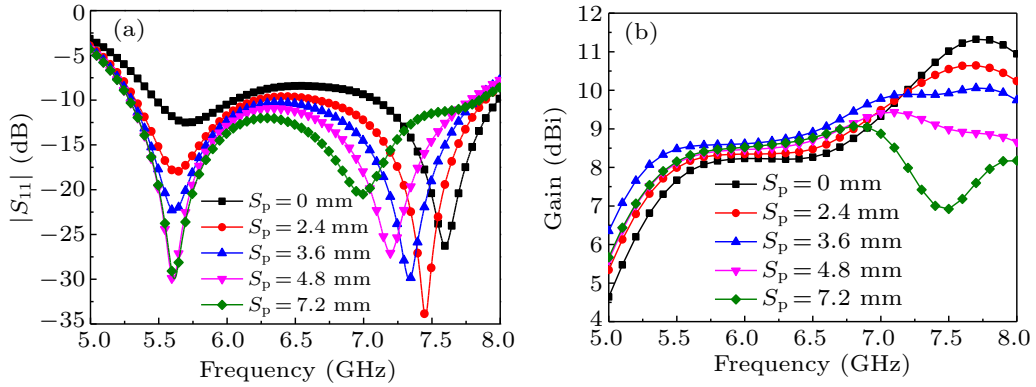


Fig. 9. Effect of S_p on antenna, showing (a) $|S_{11}|$ and (b) gain *versus* frequency.

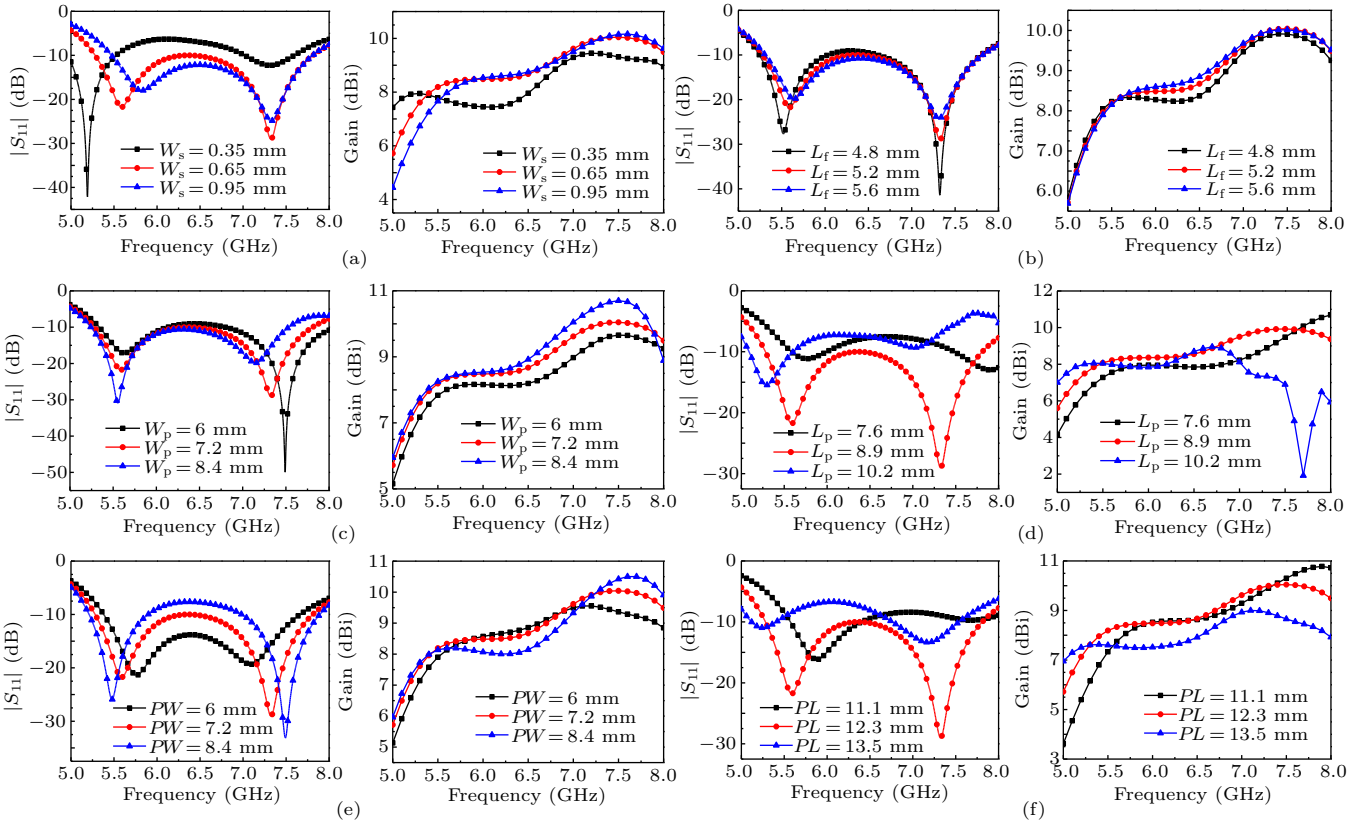


Fig. 10. Effect of W_s, L_f, W_p, L_p, PW, PL on antenna $|S_{11}|$ and gain, (a) W_s, (b) L_f, (c) W_p, (d) L_p, (e) PW, (f) PL *versus* frequency.

3.4. Parameter study

With the increase of PW, the impedance matching becomes worse, and the gain decreases at low frequency and increases at high frequency. L_f and W_p have little influence on the impedance bandwidth and gain, while W_s, L_p, and PL mainly contribute to impedance matching and gain.

4. Fabrication and measurement

The photograph of the proposed antenna and the anechoic chamber measurement environment are shown in Fig. 11. By using the full-wave simulator, HFSS 14.0 simulator, the entire antenna is simulated and characterized to derive its radiation patterns. The simulated and measured *S*-parameters and boresight gain are compared in Fig. 12, and it can be seen that the simulated pattern sidelobe is reduced at 7.5 GHz. The discrepancy between the measurements and simulations may be attributed to the ungratified experimental measurement state, the accuracy of fabrication and the accuracy of mesh generation. The measured impedance bandwidth for $|S_{11}| = -10$ dB is 39.8% (5.3 GHz–7.94 GHz), within which the boresight gain varies from 7.8 dBi to 10.04 dBi.



Fig. 11. Fabricated prototypes of proposed antenna, showing (a) top view, (b) middle patch view, (c) back view, (d) anechoic chamber measurement environment.

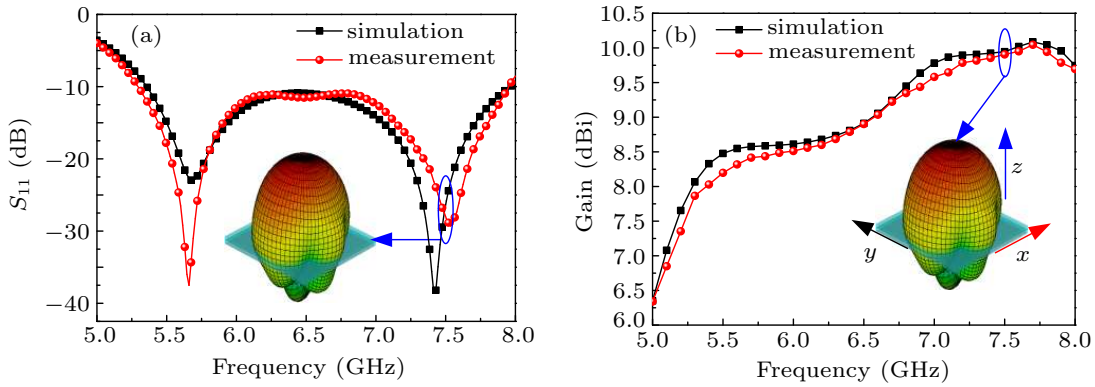


Fig. 12. Simulated (Sim.) and measured (Mea.) results of (a) return loss and (b) gain.

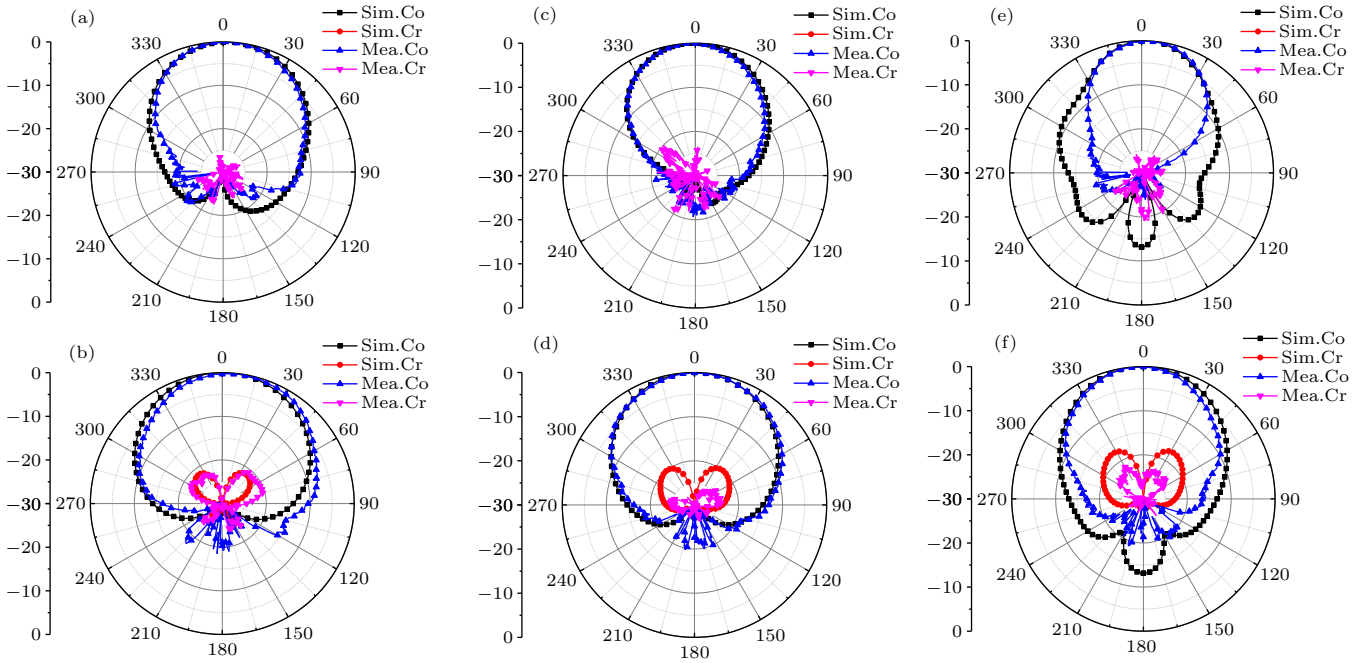


Fig. 13. Radiation patterns at (a) 5.5 GHz for *y*–*z* plane, (b) 5.5 GHz for *x*–*z* plane, (c) 6.5 GHz for *y*–*z* plane, (d) 6.5 GHz for *x*–*z* plane, (e) 7.5 GHz for *y*–*z* plane, and (f) 7.5 GHz for *x*–*z* plane.

Figure 13 shows the excellent agreement between the simulated and measured normalized radiation patterns at 5.5 GHz, 6.5 GHz, and 7.5 GHz. Besides, the measured cross-polarization levels at boresight is below −30 dB across the operating band due to the suppression of undesired modes. The performance comparison between the proposed antenna and some other metasurface antennas based on CMA are shown in Table 1.

Table 1. Comparison of wideband patch antennas based on CMA between our proposed antenna and other reported antennas.

Ref.	Size (λ_0^3)	−10-dB BW (%)	Boresight gain (dBi)
[16]	$1.01 \times 1.01 \times 0.072$	31.5	6.73–9.95
[17]	$0.95 \times 0.95 \times 0.057$	30	6.96–8.21
Proposed	$1.08 \times 1.08 \times 0.065$	39.8	7.8–10.04

5. Conclusions

A wideband high-gain and low-profile patch antenna fed by coaxial probe using metasurface is proposed, analyzed, and experimentally verified. The wideband high-gain working mechanism is well explained and understood based on the CMA. Quantities and parameters of characteristic modes effectively guid the design, optimization, and excitation placement.

References

[1] Tittl A, Leitis A, Liu M, Yesilkoy F, Choi D, Neshev D N, Kivshar Y S and Altug H 2018 *Science* **360** 1105

[2] Francesco, Aieta, Mikhail, Kats, Patrice, Genevet, Federico and Capasso 2015 *Science* **347** 1342

[3] Jia S L, Wan X, Su P, Zhao Y J and Cui T J 2016 *AIP Adv.* **6** 045024

[4] Yuan Y, Zhang K, Ratni B, Song Q, Ding X, Wu Q, Burokur S N and Genevet P 2020 *Nat. Commun.* **11** 4186

[5] Yuan Y, Sun S, Chen Y, Zhang K, Ding X, Ratni B, Wu Q, Burokur S N and Qiu C W 2020 *Adv. Sci. (Weinh)* **7** 2001437

[6] Zhang K, Yuan Y, Ding X, Li H, Ratni B, Wu Q, Liu J, Burokur S N and Tan J 2020 *Laser Photon. Rev.*

[7] Lin B Q, L-T L, Guo J X, Wang Z L, Huang S Q and Wang Y W 2020 *Chin. Phys. B* **29** 104205

[8] Zhang K, Yuan Y, Ding X, Ratni B, Burokur S N and Wu Q 2019 *ACS Appl. Mater. Interfaces* **11** 28423

[9] Zhang C, Cao X Y, Gao J and Li S J 2018 *Radioengineering* **27** 379

[10] Zhu H, Cheung S W, Chung K L and Yuk T I 2013 *IEEE Trans. Anten. Propag.* **61** 4615

[11] Zhu H, Cheung S W, Liu X and Yuk T I 2014 *IEEE Trans. Anten. Propag.* **62** 2891

[12] Zhu H, Chung K L, Sun X L, Cheung S W and Yuk T I 2012 *International symposium on antennas and propagation*, pp. 1–2

[13] Pandi S, Balanis C A and Birtcher C R 2015 *IEEE Trans. Anten. Propag.* **63** 3016

[14] Pfeiffer C and Grbic A 2015 *IEEE Trans. Anten. Propag.* **63** 3248

[15] Lin F H and Chen Z N 2018 *IEEE Trans. Anten. Propag.* **66** 1894

[16] Lin F H and Chen Z N 2017 *IEEE Trans. Anten. Propag.* **65** 1706

[17] Liang Z, Ouyang J and Yang F 2018 *J. Electromagn. Waves Appl.* **32** 2304

[18] Chen Y and Wang C F 2012 *IEEE Anten. Wireless Propag. Lett.* **11** 1474

[19] Lin J and Chu Q 2018 *IEEE Trans. Anten. Propag.* **66** 3148

[20] Zhao J, Chen Y and Yang S 2018 *IEEE Anten. Wireless Propag. Lett.* **17** 1166

[21] Garbacz and R. J 1965 *Proc. IEEE* **53** 856

[22] Harrington R F and Mautz J 1971 *IEEE Trans. Anten. Propag.* **19** 622

[23] Harrington R F and Mautz J 1971 *IEEE Trans. Anten. Propag.* **19** 629

[24] Harrington R F, Mautz J and Chang Y 1972 *IEEE Trans. Anten. Propag.* **20** 194

[25] Chang Y and Harrington R 1977 *IEEE Trans. Anten. Propag.* **25** 789

[26] Chen Y and Wang C F 2015 *Characteristic Modes: Theory and Applications in Antenna Engineering* (Hoboken, New Jersey: Wiley Publishing)

[27] Ling F, Wang C and Jin J 2000 *IEEE Trans. Microwave Theor. Techniq.* **48** 832

[28] Martens R, Safin E and Manteuffel D 2011 *Loughborough Antennas & Propagation Conference*, p. 1

[29] Martens R, Safin E and Manteuffel D 2011 *Proceedings of the 5th European Conference on Antennas and Propagation (EUCAP)*, pp. 2492–2496